Available online at www.sciencedirect.com
SCIENCE DIRECT®
Catalysis Today 102–103 (2005) 85–93
CATALYSIS TODAY
www.elsevier.com/locate/cattod

Development of methods of growing carbon nanofibers on silica glass fiber supports

Ismagilov Zinfer R. [a,*], Shikina Nadezhda V. [a], Kruchinin Vladimir N. [a], Rudina Nina A. [a], Ushakov Vladimir A. [a], Vasenin Nikolai T. [a], Veringa Hubert J. [b]

[a] *Boreskov Institute of Catalysis, Novosibirsk 630090, Russia*
[b] *ECN, P.O. Box 1, 1755 ZG Petten, The Netherlands*

Available online 24 March 2005

Abstract

Samples of carbon nanofibers (CNF) with different carbon contents (6.5–55 wt.%) are prepared by decomposition of CH_4 on Ni catalysts supported on silica glass fibers (SGF). The incipient wetness impregnation of support, introduction of the active component into alumina washcoat and ion-exchange methods were used to prepare Ni catalysts on SGF. On the optimal catalyst prepared on washcoated SGF, carbon forms as CNF of diameter 20–50 nm, and the carbon capacity is rather high—55 g_C/g_{Ni}. Diameter of the CNF corresponds to the size of catalyst particles of Ni metal, which have the cuboctahedral form typical for the formation of CNF with conical embedding of graphite layers with respect to the filament axis. The SGF with supported CNF is a mesoporous material with polydisperse pore distribution similar by structural and textural parameters to the granulated bulk CNF obtained in methane decomposition over high-loaded nickel-alumina catalysts.

The XRD, ESR and DTA methods were used for phase and structural analysis and demonstrated that CNF has a uniform graphite-like structure and does not include the amorphous phase.
© 2005 Published by Elsevier B.V.

Keywords: Structured supports; Carbon; Carbon nanofibers; CNF; Silica glass fiber; Methane decomposition

1. Introduction

Carbon nanofibers (CNF) can be produced as powder or granules via the decomposition of hydrocarbons, in particular methane, over catalysts composed of iron group metals [1–3] and oxides Al_2O_3, SiO_2, etc. For practical application, it is of interest to grow carbon filaments on the organized geometrical surface of structured materials [4,5], for instance, on honeycomb monoliths, reticulated foam materials, porous composite ceramics, woven and non-woven ceramic fibers.

Of special interest are glass fibers, due to physico-chemical properties of glass fiber in metastable amorphous state [6] and a high total geometrical surface area of macrostructured fibrous materials composed of thin elementary fibers. Besides, glass fibers exhibit high strength, they can be easily transformed to required geometric shape, which enhances the integration of catalysts into reactors of various space geometry. These advantages of glass fiber materials can be enhanced for preparation of catalyst supports by depositing carbon nanofibers layer with developed mesoporous structure.

Carbon nanofibers can be grown by the catalytic decomposition of hydrocarbons over nanodispersed metal catalysts loaded on the surface, e.g., on glass fibers. We summarized the known methods of active metal catalyst loading onto glass fibers into four groups:

1. Capillary incipient wetness impregnation of glass fiber with solutions of precursors [7].
2. Introduction of the active component by the impregnation method into preliminary formed oxide layer on the surface of glass fibers [8,9].
3. Impregnation by the ion-exchange method [10].
4. Introduction of active metals into the raw mix for glass fiber production, followed by their supporting with conventional methods [11].

* Corresponding author. Tel.: +7 3832 341219; fax: +7 3832 397352.
E-mail address: zri@catalysis.nsk.su (I.Z. R.).

0920-5861/$ – see front matter © 2005 Published by Elsevier B.V.
doi:10.1016/j.cattod.2005.02.009

In the present work, methane decomposition catalysts were prepared by methods 1–3.

The effects of preparation procedure on the properties of Ni-containing catalysts and their activity in methane decomposition have been determined.

Time of operation until deactivation for each supported catalyst and morphology of CNF were studied.

Structural and textural properties of CNF grown on glass fibers coated with a catalyst of optimum composition were investigated.

2. Experimental

2.1. Support

Silica glass fibers (SGF) used in experiments consists of filaments with a diameter of 6–7 μm (Fig. 1). After removal of a lubricant, the glass fiber was leached in a 5.5% solution of nitric acid for 1 h at 90 °C, washed with water to obtain pH 5.5–7, dried and calcined at 300 °C in air. The properties of SGF after pretreatment are as follows: S_{BET}^{Ar} is 0.7 m^2/g, $S_{BET}^{N_2}$ is 0.3 m^2/g, V_{pore} is 0.00056 cm^3/g, amorphous phase in XRD.

2.2. Catalysts

The Ni-containing catalysts supported onto SGF were prepared by three methods. In all cases, an aqueous solution of nickel nitrate was used as the active component precursor.

According to method 1 (catalyst 1), the active component was introduced via the incipient wetness impregnation of SGF itself at room temperature. Then the samples were separated from the impregnating solution, dried at 70 °C, calcined at 350 °C in nitrogen, and reduced in a mixture of 10 vol.% H_2 + 90 vol.% N_2 at 550 °C for 3 h. The Ni content in the catalyst was 4.2–4.5 wt.%.

By method 2 (catalyst 2), the active component was fixed in the alumina layer (0.75 wt.% alumina with respect to SGF) formed on SGF from a solution of aluminum nitrate. After separation of the impregnating solution, the samples were heat treated in the regime similar to that of method 1. The Ni content in the catalyst was 2.2–2.4 wt.%.

According to method 3 (catalyst 3), samples of the support were boiled in a precursor solution for 1 h, then the samples were separated from the solution, washed with distilled water to remove Ni cations weakly bonded to the support and treated under the conditions similar to those of methods 1 and 2. The Ni content in the catalyst was 0.02 wt.%.

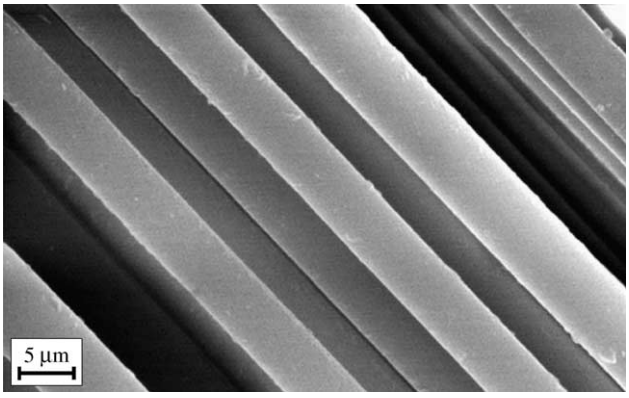

Fig. 1. The micrograph of SGF fibers.

2.3. Characterization

Chemical composition of the support and catalysts was determined by the method of atomic-emission spectroscopy with inductively confined plasma using a BLYRD spectrometer.

Carbon content in the samples was measured gravimetrically from the sample weight increment and weight loss after burning at 1000 °C. In some cases, thermogravimetric analysis (TGA) was used. TGA and DTA were performed in air at a heating rate 10°/min and a temperature range from 22 to 1000 °C with 100 mg samples.

Adsorption methods were used for characterization of the textural properties of support, catalysts and carbonized samples of glass fibers. The value of specific surface area was determined by the BET method from heat desorption of argon, S^{Ar}, and nitrogen adsorption at 77 K. Pore volume and pore size distribution were also determined from nitrogen adsorption at 77 K with an ASAP-2400 instrument. Effective pore diameter was found from the differential curve plotted with the data obtained by the Barrett–Joyner–Halenda method using the model of cylindrical pores. Average pore radius was calculated by the formula $4V/S_{BET}$.

Phase composition of support and catalysts, and size of the active component particles (coherent scattering region, c.s.r.) were determined by analyzing the diffraction patterns in the range of 2θ angles from 10 to 60° obtained with a HZG-4 diffractometer at monochromatic Cu Kα radiation. The structure of carbon nanofibers was characterized by d_{002} and c.s.r. in the directions perpendicular to the basal plane (L_c) and along it (L_a).

The degree of graphitization was determined according to [12] from the formula: $g = (0.344 - d_{002})/0.0086$.

Morphology of supports, catalysts and carbonized samples of glass fibers was studied by the SEM and TEM methods with microscope REM 100-U and a transmission electron microscope JEM-100CX. Samples for the TEM studies were pounded with a pestle, suspended in ethanol, then dispersed by ultrasound and fastened to copper nets.

The ESR studies of catalysts and carbon coating were performed with a Bruker ER 200D spectrometer (λ = 3 cm) at 77 and 300 K. Values of the ESR parameters were found by comparing with the position of the diphenylpicrylhydrazyl (DPPH) line.

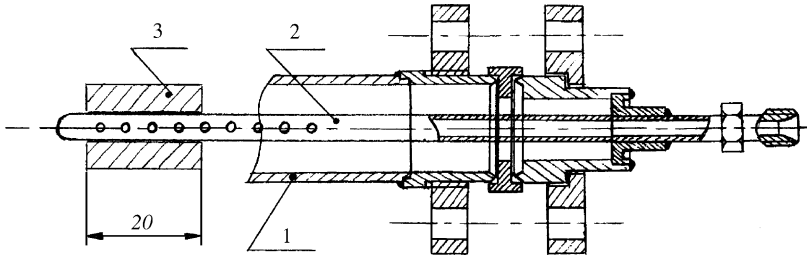

Fig. 2. The flow reactor: (1) reactor wall; (2) gas distributing tube; (3) catalyst on glass fiber support.

2.4. Methane decomposition and CNF growing

The methane decomposition reaction was performed in a horizontal flow reactor. The 20 mm tape of silica glass fiber containing supported Ni catalyst was rolled in a 20 mm diameter coil on a perforated metal tube operating as a gas distributor (see Fig. 2). The reaction mixture consisting of 25 vol.% natural gas (98% methane + trace amounts of ethane and propane) and 75 vol.% N_2 was fed into the reactor at a space velocity of 2500 h^{-1}. The reaction mixture (CH_4, N_2, H_2, hydrocarbons) was analyzed with GC. The experiments were performed at 550 °C until complete deactivation of a catalyst. Activity of catalysts in methane decomposition was characterized by methane conversion (X_{CH_4}), catalyst lifetime (time of its operation until a complete deactivation, τ_{cat}) and carbon capacity (G_C).

Methane conversion was calculated by the formula [13]:

$$X_{CH_4} = \frac{(C_0 - C)}{C_0(1 + C)} 100\%$$

where C_0 is the mole fraction of methane in the initial reaction mixture; C is the mole fraction of methane in the reaction products.

Carbon capacity of the catalysts was determined as the ratio of carbon weight in the carbonized catalyst sample to the weight of Ni in the catalyst.

3. Results and discussion

To reveal the degree of reduction of the active component and the size of its particles in catalysts prepared by different methods, structural and textural properties of the catalysts were studied using the ESR, XRD, nitrogen adsorption and scanning microscopy methods.

ESR studies of catalysts were performed after their reduction in hydrogen. ESR spectra are observed only for catalysts 1 and 2. The observed spectra have broad lines, exceeding 2000 Gs at room temperature, and show a further broadening at the temperature of liquid nitrogen. All these observations clearly indicate that the spectra correspond to ferromagnetic (superparamagnetic) particles of nickel metal Ni^0. Catalyst 3 has no ESR signals spectra both at room temperature and at 77 K, which evidences that nickel atoms are in a different electron state as compared to the first two catalysts.

The XRD data are presented in Table 1 and in Fig. 3. Before the reduction stage, the diffraction pattern of catalysts 1 and 2 is characterized by a mixture of two phases: X-ray amorphous phase of support and nickel oxide phase represented by the 2θ reflexes at 37.5 and 43.5°. The size of the nickel oxide particles determined from the coherent scattering region is 14 nm in catalyst 1 and 7 nm in catalyst 2. After heat treatment in H_2, the reflexes corresponding to NiO phase disappear from the diffraction pattern, and the 2θ maxima are observed at 44.5 and 52°, which are typical of the Ni metal phase with the particle size 20 and 16 nm, respectively, for catalysts 1 and 2. The size of Ni particles determined from the c.s.r. is an averaged characteristic. In catalyst 1, the reflexes corresponding to nickel metal phase have the profile (a broad base passing to a narrow peak) typical of polydisperse size distribution of Ni particles, which indicates that the catalyst comprises metal particles considerably differing in size.

In catalyst 2, a uniform size distribution of Ni particles is observed. Diffraction pattern of catalyst 3 sample after its calcining at 350 °C in nitrogen before the reduction stage and after heat treatment at 550 °C in hydrogen flow is identical to the diffraction pattern of amorphous glass fiber support represented by an extended hallo in the 2θ range of 22–23°. This result is obvious considering very low (0.02 wt.%) Ni content.

Catalysts 1 and 2 after heat treatment in N_2 have close values of textural parameters: the total pore volume, specific

Table 1
XRD data for Ni catalysts on glass fiber support

Catalyst type	Ni content (wt.%)	Heat treatment in N_2 (350 °C)		Heat treatment in H_2 (550 °C)	
		Phase	c.s.r. (nm)	Phase	c.s.r. (nm)
1	4.5	NiO, amorphous phase	14	Ni amorphous phase	20
2	2.2	NiO, amorphous phase	7	Ni amorphous phase	16
3	0.02	Amorphous phase	–	Amorphous phase	–

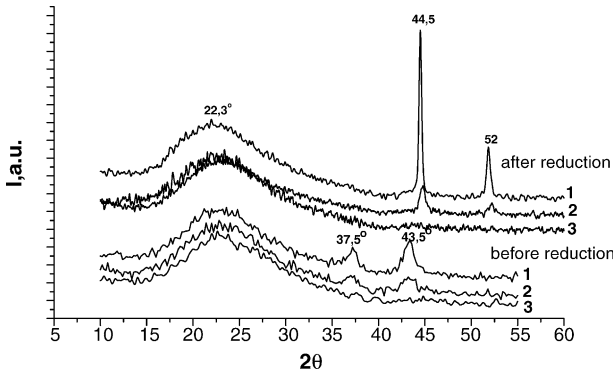

Fig. 3. XRD patterns of catalysts 1, 2 and 3 before and after the reaction.

surface area and effective pore radius (Table 2). After reduction at 550 °C, transformation of NiO to Ni occurs, and the specific surface area and pore volume decrease. This effect is more pronounced for catalyst 1. The decrease of the surface area is 10-fold while the measured particle size decreases only by a factor of 1.4 can be explained by the presence in this catalyst of large Ni particles in addition to smaller particles with an average size of 20 nm. Indeed, the determination of particle size over 50 nm cannot be performed by c.s.r. method used, and their presence in the catalyst sample may cause the observed sharp decrease of the SSA and pore volume values.

The presence of the alumina washcoating layer in catalyst 2 favors the stabilization of its textural parameters.

Textural properties of catalyst 3 are virtually similar to the properties of glass fiber ($S_{BET} = 0.3$ m^2/g, $V_{pore} = 0.00056$ cm^3/g).

Fig. 4 displays the electron micrographs demonstrating surface morphology of catalysts 1 (Fig. 4(1a)) and 2 (Fig. 4(2a)). In catalyst 1, the active component forms as coarse crystallites distributed over the external surface of glass fibers. One may expect a weak interaction between the active component and support. In catalyst 2, particles of the Ni active component are bonded rather strongly to alumina supported onto the surface of glass fibers.

It is known that alumina is a textural promoter in methane decomposition catalysts, on the one hand, providing the dispersity of catalytic particles (15 nm for Ni-Al catalyst) necessary for the carbon capacious state, and on the other hand, preventing the particles merging [14]. Table 3 presents the data on the initial degree of methane conversion, carbon capacity and lifetime of the catalysts prepared by various methods. It can be seen from these data that the catalysts exhibit considerably different activity in methane decomposition. At the initial moment, similar and rather high degrees of methane conversion (35–38%) on catalysts 1 and 2 are observed. High initial activity of these catalysts may be due to the presence of high-dispersed Ni particles (according to the XRD data) with an optimum size for the reaction. Methane decomposition does not occur on catalyst 3 obtained by the ion-exchange method due to the lack of Ni metal particles (according to the ESR data) on which the growth of carbon nanofibers occurs.

Table 2
Textural characteristics of catalysts obtained by methods 1 and 2

Catalyst	Heat treatment	$D^{ef.}_{pore}$ (nm)	D_{pore} average (nm)	S_{BET} (m^2/g)		V_{pore} (cm^3/g)
				Ar	N_2	
1	In N_2, 350 °C	3.5	5.2	8.1	7.9	0.01
2	In N_2, 350 °C	3.5	6.4	6.7	5.8	0.01
1	In H_2, 550 °C	9.5	16.7	0.9	0.62	0.0026
2	In H_2, 550 °C	3.5	9.6	4.4	3.4	0.0082

Fig. 5 shows the dependence of methane conversion on the reaction time. Catalyst 1 deactivates quite rapidly; 30 min after the reaction onset its activity drops sharply, and the reaction ceases in 3 h. Two periods of steady operation are observed on catalyst 2 (their total time is 120 min), the reaction proceeding with high methane conversion, then a gradual deactivation of the catalyst starts. The catalysts differ not only in their lifetime but also in the amount of carbon formed.

In catalyst 1, a weak interaction of the active component with the support, on the one hand, facilitates the detachment of metal particles from the support surface causing growth of carbon filaments unattached to the support; on the other hand, it favors the enlargement of Ni particles up to 400 nm (Fig. 4(1b)) during the reaction. The enlargement of Ni particles to this size may result in their partial peeling from the surface of glass fiber or incapsulation by carbon deposits, causing fast deactivation of the catalyst. Fig. 4(1b) displays the micrograph of carbonized sample of catalyst 1 after 30 min operation. Along with carbon filaments of thickness 25–70 nm, this sample contains 200–500 nm metal particles incapsulated by carbon. The active component of catalyst 2, uniformly distributed in the secondary washcoating alumina layer, is composed of particles ∼16 nm in size, which are enlarged to the size about 50 nm during methane decomposition (Fig. 4(2b)). Probably, this is the optimal size, providing a longer catalyst operation as compared to catalyst 1.

Morphology of catalysts affects also the macrotextural properties of the formed CNF. Even at the initial period of the reaction (30 min after the onset) at a low CNF content ($C_{CNF} \sim 10\%$), carbon filaments forming on catalyst 1 virtually "hang" in the space between the glass fibers (Fig. 4(1c)). In the case of catalyst 2, the washcoat holds carbon fibers on its surface, preventing their detachment into the interfibrillar space (Fig. 4(2c), $C_{CNF} \sim 10\%$). This effect is most pronounced at high carbon contents in the samples. Fig. 4(1d) presents the micrograph of catalyst 1 sample containing 15 wt.% CNF, which shows that carbon filaments are arranged separately from glass fibers. For catalyst 2, the detectable carbon coating detachment from the fiber surface occurs only at a rather high carbon content. This is demonstrated in Fig. 4(2d) for the sample with 24 wt.% CNF content.

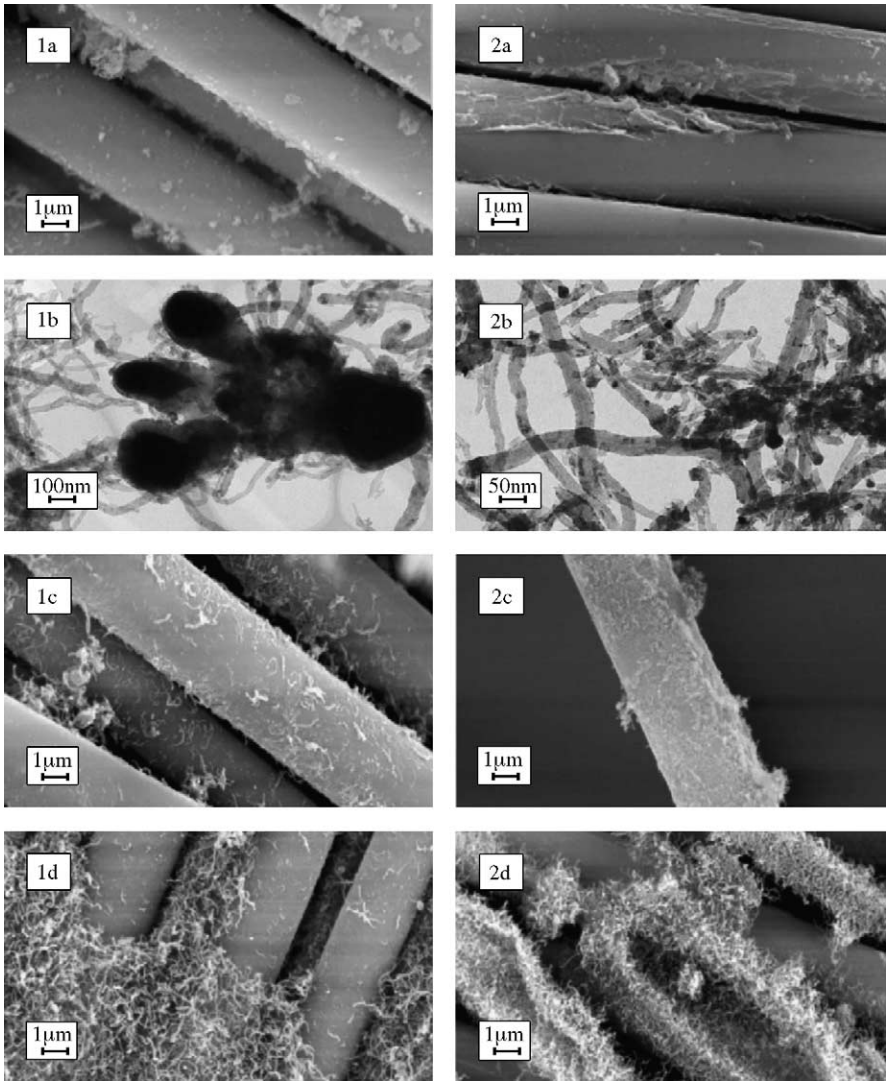

Fig. 4. The micrographs of catalysts 1 and 2 before and after the reaction: (1a) catalyst 1; (1b) CNF/cat. 1 (TEM); (1c) 10% CNF/cat. 1; (1d) 15% CNF/cat. 1; (2a) catalyst 2; (2b) CNF/cat. 2 (TEM); (2c) 10% CNF/cat. 2; (2d) 24% CNF/cat. 2.

4. Properties of CNF

The samples of CNF on catalyst 2 were taken for further physico-chemical studies. Depending on the reaction time, the samples contain different amounts of CNF (Table 4).

4.1. XRD

The size of Ni particles, determined from the coherent scattering region, changed from 16 nm for the initial catalyst

Table 3
Methane conversion, lifetime and carbon capacity of catalysts prepared by different methods

Catalyst	Ni (wt.%)	$X^0_{CH_4}$ (%)	τ_{cat} (h)	G_C (gC/gNi)
1	4.5	35	3	8.3
2	2.2	38	5.7	55
3	0.02	0	0	0

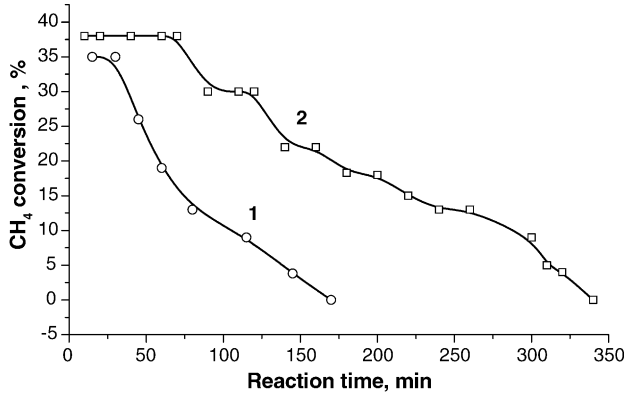

Fig. 5. The dependencies of methane conversion on the reaction time and preparation procedure (methods 1 and 2).

Table 4
List of samples prepared on catalyst 2

Sample code	CNF content (wt.%)	Reaction time (min)
2.1	6.5	15
2.2	10	25
2.3	24	60
2.4	55	350

to 20 nm after 15 min (sample 2.1), 35 nm after 25 min (sample 2.2) and 40 nm after 60 min (sample 2.3) of the reaction. The Ni metal phase is not detected in sample 2.4, since dilution of the sample with carbon decreases the nickel concentration by a factor of 2, making it lower than the sensitivity of the method. Carbon phase is detected in the samples with carbon content exceeding 10 wt.%. Diffraction pattern of sample 2.3 shows the maxima corresponding to three phases: X-ray amorphous phase of support at 22.3°; Ni metal phase at 44.5 and 52°, size 40 nm; and carbon phase with the maximum at 26°. Characteristics of the carbon structure ordering were determined only for the sample with the CNF concentration of 55 wt.%. Diffraction pattern of sample 2.4 corresponds to a nearly pure carbon phase, which is characterized by a local ordering in the structure of adjacent layers, parameter $L_c = 3.9$ nm, and by a local ordering within each layer, parameter $L_a = 6.9$ nm, which is much smaller than the diameter of filament. Interlayer distance d_{002} is 0.343 nm, and degree of graphitization (g) calculated from this parameter is 0.116. These parameters are close to those found for the turbostratic structure of granulated CNF synthesized under similar conditions ($L_c = 4.3$ nm; $L_a = 6.2$ nm; $d_{002} = 0.343$ nm) [15].

4.2. TEM

Fig. 6 displays the micrograph of carbonized fiber sample taken 1 h after the reaction onset (sample 2.3). Morphology of the carbon phase is presented by filaments 20–50 nm thick, corresponding to the size of metal particles. Ni metal particles have the cuboctahedral form typical for the

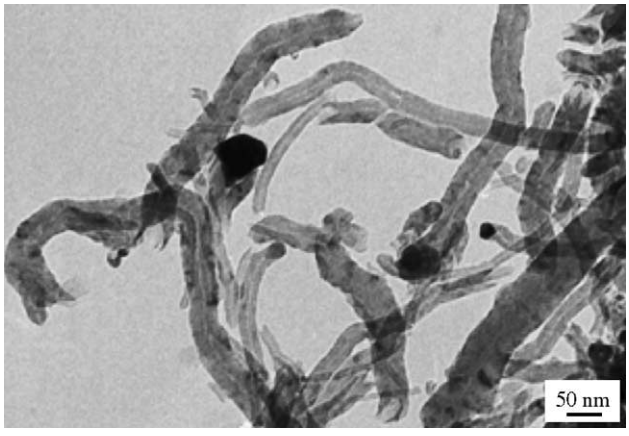

Fig. 6. Carbon nanofibers with Ni particles.

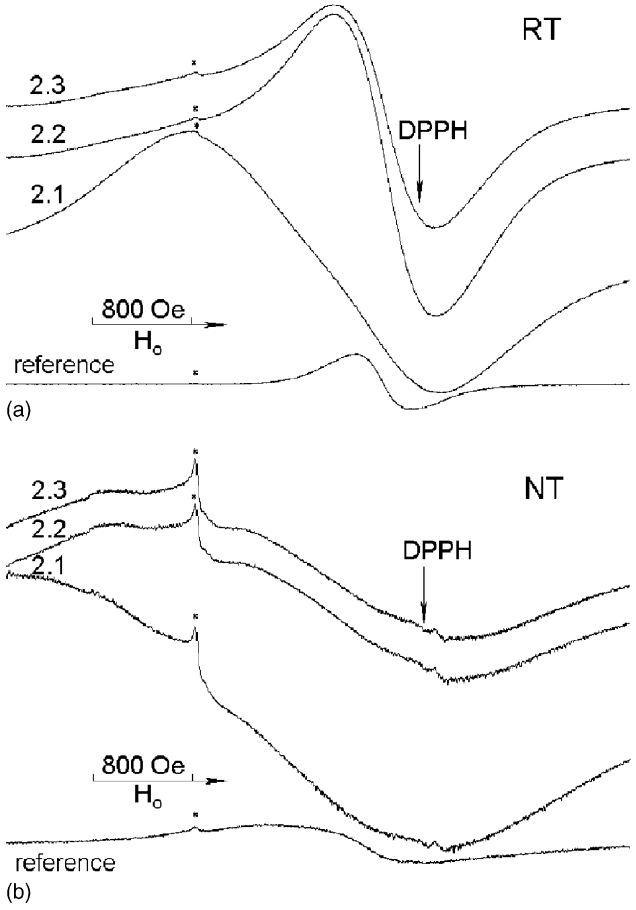

Fig. 7. ESR spectra of the samples with different CNF content: 2.1–6.5%, 2.2–10%, 2.3–24%, ref. – granulated CNF (a) at room temperature; (b) at 77 K.

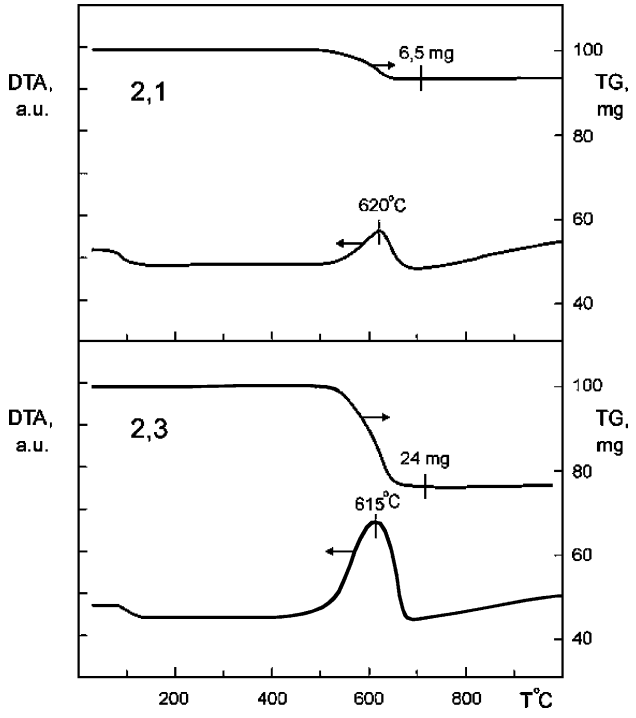

Fig. 8. DTA and TG curves of the samples: 2.1–6.5% CNF; 2.3–24% CNF.

Table 5
Textural properties of CNF on SGF after methane decomposition at different reaction times

Sample code	Reaction time (min)	CNF (wt.%)	$D_{pore}^{ef.}$ (nm)	$D_{pore}^{average}$ (nm)	V_{pore} (cm^3/g)	S_{BET} (m^2/g)	Size distribution of pore volume	
							(nm)	(%)
2.1	15	6.5	3.6	4.64	0.01	4.8	3.0–7.0	50
							7.0–12.0	7.5
							12.0–17.5	5
							>17.5	37.5
2.3	60	24	3.6	7.43	0.035	19	3.0–7.0	17
							7.0–12.0	14
							12.0–17.5	14
							>17.5	55
2.4	350	55	3.6; 12.0	10.64	0.138	51.7	3.0–7.0	10
							7.0–12.0	12
							12.0–17.5	18
							>17.5	60

formation of CNF with conical arrangement of graphite layers with respect to the filament axis [15].

4.3. ESR

XRD data showed that CNF that forms during CH_4 decomposition in the samples under study has a graphite-like structure. The experimentally obtained value $d_{002\ carbon} = 0.343$ nm exceeds the interplanar distance for ideal graphite ($d_{002\ graphite} = 0.335$ nm). It means that the structure of the formed carbon has only a local ordering and does not exclude the presence of the graphite structure defects. Presumably, different steps of the reaction yield carbon with different degree of structural ordering. It is not improbable that samples comprise a small amount of amorphous carbon (as coke). Coke is known to contain a large amount of paramagnetic sites, so the ESR method was used to study the samples after methane decomposition at different reaction times. Samples 2.1, 2.2 and 2.3 were used in these experiments. The samples contain ~2 wt.% Ni. Granulated CNF prepared on 90% Ni–Al_2O_3 and containing 0.18% Ni was used as the reference sample. ESR spectra were taken at room temperature (Fig. 7a) and at the temperature of liquid nitrogen (Fig. 7b). Spectral lines of samples are very broad (the width of the narrowest line is ~800 Gs) and cannot be assigned to the ESR spectra of coke, which has the g-factor equal to $g_e = 2.0023$ and the line width of 1–7 Gs. The ESR spectrum of granulated CNF differs from the above spectra only in a lower intensity of the lines. All the lines observed can be assigned to the ESR spectra of Ni^0 ferromagnetic particles. It was assumed that ferromagnetic nickel particles affect the paramagnetic pattern of coke and cause the line broadening. To exclude the effect of Ni, the samples were washed by boiling in a 3 M solution of hydrochloric acid, followed by repeated washing with distilled water to remove Cl^- ions. Ni content in the samples decreased approximately by a factor of 7. ESR spectra of the washed samples showed a much lower intensity of the lines, but no ESR spectra of coke were observed.

The effect of oxygen is well known from the literature on ESR studies of coke [16]. This effect is represented by broadening of the ESR spectra of coke at adsorption of small amounts of molecular oxygen. So, air was pumped out from the ampoules with samples at 250 °C to pressure 10^{-2} Torr. After removal of oxygen, ESR spectra did not change. The obtained data indicate that the ESR spectra of coke are absent in the samples studied irrespective of the degree of magnetism of nickel particles and the presence of oxygen. Therefore, it can be assumed that the formed CNF in the samples studied are of graphite-like structure, containing degenerated electron gas (the occurrence of electron conduction). It is known that in this case, electron gas is connected with localized paramagnetic sites of the graphite-like structure by exchange interaction, which leads to considerable broadening of ESR spectra of these sites.

4.4. TGA and DTA

Carbon species of different nature burn out at different temperatures, so the samples of CNF on glass fibers (2.1 and 2.3) obtained after 15 and 60 min of methane decomposition were studied by DGA and DTA. An exoeffect is observed at 615–620 °C in the DTA curves of samples 2.1 and 2.3

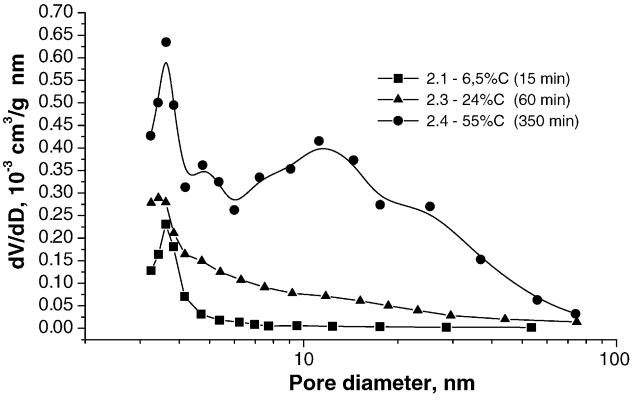

Fig. 9. Pore size distribution for the samples with different CNF content.

Table 6
Effect of treatment of CNF on SGF in neutral and acid media

Treatment conditions	Ni content in the initial sample (wt.%)	Ni content in the washed sample (wt.%)	Washing degree (%)	C content in the initial sample (wt.%)	C content in the washed sample (wt.%)	Carbon losses (%)
1) In H_2O at 100 °C for 10 h	2.3	Not determined	Not determined	23.3	22.9	1.7
2) In 3 M HCl at 100 °C for 10 h	2.3	0.3	87	23.3	21.8	6.4
3) In H_2SO_4 at 20 °C for 150 h	2.3	0.1	95.6	23.3	20.5	12.0

(Fig. 8). The absence of other peaks is an indirect evidence of the uniform composition of CNF. TGA was used for the determination of CNF content in samples.

4.5. Textural properties

Nitrogen adsorption isotherms at 77 K, obtained at measuring the textural properties CNF grown on SGF, form the capillary-condensation hysteresis loop, which is assigned to the H-3 type according to the IUPAC classification. The H-3 type loop is typical for mesoporous materials with predominating slit-like pores. Textural properties of CNF on SGF depend on the diameter of formed carbon filaments and their orientation in space relative to each other and to glass fibers. As the reaction proceeds, the size of Ni particles changes, and so does the thickness of carbon filaments. Thus, one may expect the textural parameters of the forming carbon phase to change with increasing reaction time. Textural properties of the samples with different CNF content obtained in 10 min, 1 and 6 h after the reaction onset are presented in Table 5. Fig. 9 shows the differential pore size distribution.

An observed increase in the total pore volume and specific surface area of the samples with increasing reaction time is obviously caused by the increased amount of mesoporous carbon phase.

Differential curves of the pore size distribution (Fig. 9) show the maximum at 3.6 nm for all samples. As the reaction time increases, broadening of the forming pores occurs. Filaments of different thickness can entangle or grow into the interfibrillar space, ultimately forming the porous structure with polydisperse pore distribution.

From the values of V_{pore} and S_{BET} for CNF and the same values for the initial catalyst, the pore volume and specific surface area of the carbon phase can be calculated: V_{pore} = 0.245 cm^3/g; S_{BET} = 94 m^2/g (sample 2.4). These values are close to those obtained for bulk CNF synthesized under similar conditions over the 90% Ni 10% Al_2O_3 catalyst (V_{pore} = 0.22 cm^3/g; S_{BET} = 109 m^2/g; D_{pore} = 10.8 nm) [15].

4.6. Stability of CNF on SGF

Samples of carbonized catalysts on glass fibers contain nickel particles. To prepare catalysts on carbon support or to modify functional groups on the carbon surface, the samples are treated with mineral acids for removing the metal particles. In such cases, of great importance is the stability of carbon coating to losses caused by the action of aggressive media under hydrothermal conditions. Results of treatment of carbonized samples under various conditions are presented in Table 6. It is seen that practically no carbon is removed if the treatment is performed in neutral medium. Boiling in a diluted hydrochloric acid or long treatment by concentrated sulfuric acid results in minor carbon losses, which may be caused by partial dissolution of the glass fiber components and peeling of carbon filaments weakly bonded to the surface.

5. Conclusion

Samples of CNF with different carbon content (6.5–55 wt.%) were prepared by decomposition of CH_4 on supported Ni catalysts. The influence of the preparation method of Ni catalysts on their properties and activities in methane decomposition was studied. The alumina coating in catalyst 2 was shown to stabilize its textural parameters and lead to the formation of the active component state with an optimum size of Ni particles providing a high carbon capacity of the catalyst.

The X-ray diffraction analysis showed that the obtained CNF has a graphite-like structure with the following parameters: d_{002} = 0.343 nm, L_c = 3.9 nm and L_a = 6.9 nm. The ESR and DTA methods demonstrated that the CNF has a uniform structure and does not include the amorphous phase. According to the ESR data, carbon has a graphite-like structure with electron conduction.

Carbon forms as filaments of diameter 20–50 nm. The diameter of the filaments corresponds to the size of catalytic particles of Ni metal, which has the cuboctahedral form typical for the formation of CNF with conical embedding of graphite layers with respect to the filament axis.

According to the nitrogen adsorption data, CNF is a mesoporous material with polydisperse pore distribution. It was revealed that the values of structural and textural parameters of CNF grown on glass fiber supports are close to those of granulated CNF obtained in methane decomposition over high-loaded nickel-alumina catalysts.

References

[1] J.R. Rostrup-Nielsen, D.L. Trimm, J. Catal. 48 (1977) 155.
[2] K.P. De Jong, J.W. Geus, Catal. Rev. 42 (4) (2000) 481.

[3] L.B. Avdeeva, T.V. Reshetenko, Z.R. Ismagilov, V.A. Likholobov, Appl. Catal. A 228 (2002) 53.
[4] C. Pham-Huu, N. Keller, L.J. Charbonniere, R. Ziessel, M.J. Ledoux, Chem. Commun. (2000) 1871.
[5] Th. Vergunst, F. Kapteijn, J.A. Moulijn, Carbon 40 (2002) 1891.
[6] V.V. Barelko, P.I. Khalzov, S.M. Baturin, et al., RU Patent 2081898 (1994).
[7] I. Yuranov, L. Kiwi-Minsker, M. Slin ko, E. Kurkina, E.D. Tolstunova, A. Renken, Chem. Eng. Sci. 55 (2000) 2827.
[8] V. Höller, I. Yuranov, L. Kiwi-Minsker, A. Renken, Catal. Today 69 (2001) 175.
[9] F. Reinone, L. Kivi-Minsker, D.A. Bulushev, Ph.A. Buffat, A. Renken, Appl. Catal. A 244 (2003) 251.
[10] V.V. Barelko, B.S. Balzhinimaev, C.P. Kildyashev, et al., US Patent 0082088 (2003).
[11] V.V. Barelko, P.I. Khalzov, V.N. Zvyagin, et al., RU Patent 2069584 (1994).
[12] J. Mering, J.J. Maire, Chem. Phys. 57 (1960) 803.
[13] K. Hedden, S. Ruch, Chem. Eng. Technol. 39 (1967) 1017.
[14] O.V. Goncharova, L.B. Avdeeva, V.B. Fenelonov, et al. Kinet. Catal. 36 (1995) 268.
[15] T.V. Reshetenko, L.B. Avdeeva, Z.R. Ismagilov, et al. Carbon 41 (2003) 1605.
[16] A.A. Shklyaev, V.F. Anufrievko, L.M. Vasilieva, DAN SSSR 200 (No. 5) (1971) 1165.